Fe(III) Coordination Properties of Two New Saccharide-Based Enterobactin Analogues: Methyl 2,3,4-Tris-*O*-{*N*-[2,3-di(hydroxy)benzoyl-glycyl]-aminopropyl}-α-D-glucopyranoside and Methyl 2,3,4-Tris-*O*-{*N*-[2,3-di-(hydroxy)-benzoyl]-aminopropyl}-α-D-glucopyranoside

Suraj Dhungana,[†] Susanne Heggemann,[‡] Lothar Heinisch,[‡] Ute Möllmann,[‡] Hakim Boukhalfa,[†] and Alvin L. Crumbliss*,[†]

Department of Chemistry, Duke University, Box 90346 Durham, North Carolina 27708-0346, and Hans Knöll-Institut für Naturstoff-Forschung, Jena, Germany

Received April 16, 2001

The synthesis of two saccharide-based enterobactin analogues, methyl 2,3,4-tris-*O*-{*N*-[2,3-di(hydroxy)benzoyl-glycyl]-aminopropyl}-α-D-glucopyranoside (H_6L_A) and methyl 2,3,4-tris-*O*-{*N*-[2,3-di(hydroxy)benzoyl]-amino-propyl}-α-D-glucopyranoside (H_6L_B), are reported along with their pK_a values, Fe(III) binding constants, and aqueous solution speciation as determined by spectrophotometric and potentiometric titration techniques. Use of a saccharide platform to synthesize a hexadentate triscatechol chelator provides some advantages over other approaches to enterobactin models, including significant water solubility, resistance to hydrolysis, and backbone chirality which may provide favorable recognition and availability to cells. The protonation constants for the catechol ligand hydroxyl moieties were determined for both ligands and found to be significantly different, which is attributed to the differences in the spacer chain of the two triscatechols. Proton dependent Fe(III)−ligand equilibrium constants were determined using a model involving the sequential protonation of the Fe(III)−ligand complex. These results were used to calculate the formation constants, log $\beta_{110} = 41.38$ for Fe(III)−H_6L_A and log $\beta_{110} = 46.38$ for Fe(III)−H_6L_B. The calculated pM values of 28.6 for H_6L_A and 28.3 for H_6L_B indicate that these ligands possess Fe(III) affinities comparable to or greater than other enterobactin models and are thermodynamically capable of removing Fe(III) from transferrin.

Introduction

Iron is the most abundant transition metal found in the biosphere and is essential for the growth of almost all living organisms.[1] Iron in its most common form, Fe(III) hydroxide, is not a readily available nutrient since its solubility product is only 10^{-38} M^4.[2] Microorganisms, in particular, have developed a sophisticated Fe(III) acquisition and transport system involving siderophores, low molecular weight chelating agents that bind Fe(III) ion with high specificity. These potent and specific chelators usually include either catecholate or hydroxamate functional groups for iron coordination.[3−8] Enterobactin (Figure 1), a naturally occurring triscatechol, is the most powerful Fe(III) chelator known with an overall stability constant of 10^{49}.[9]

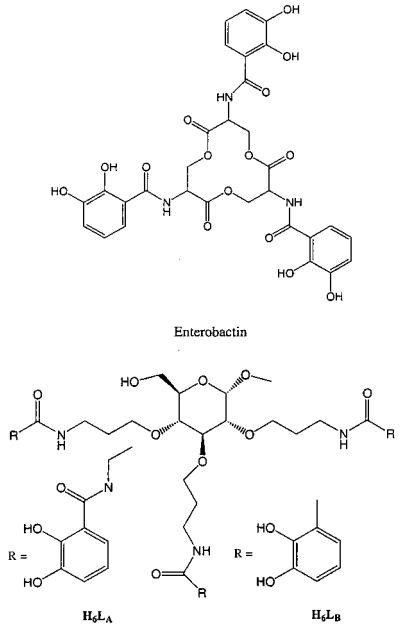

Figure 1. Enterobactin, a potent naturally occurring siderophore with catechol functional groups and two synthetic siderophore analogues with a saccharide backbone: methyl 2,3,4-tris-*O*-{*N*-[2,3-di(hydoxy)-benzoyl-glycyl]-aminopropyl}-α-D-glucopyranoside (H_6L_A) and methyl 2,3,4-tris-*O*-{*N*-[2,3-di(hydoxy)-benzoyl]-aminopropyl}-α-D-glucopyranoside (H_6L_B).

Microbial iron acquisition from the environment involves three steps: solubilization (chelation) of Fe(III) from its highly insoluble hydroxide form; transport to and across the cell

* Address correspondence to this author. E-mail: alc@chem.duke.edu. Fax: (919) 660−1605.
† Duke University.
‡ Hans Knöll-Institut für Naturstoff-Forschung.

(1) Crichton, R. R. *Inorganic Biochemistry of Iron Metabolism*; Ellis Horwood: West Sussex, England, 1991.
(2) Skoog, D. A.; West, D. M. *Fundamentals of Analytical Chemistry*, 3rd ed.; Holt, Reinhart, and Winston: New York, 1976.
(3) Crumbliss, A. L. In *Handbook of Microbial Iron Chelates*; Winkelmann, G., Ed.; CRC Press: Boca Raton, FL, 1991; pp 177−233.
(4) Albrecht-Gary, A.-M.; Crumbliss, A. L. In *Metal Ions in Biological Systems*; Sigel, A., Sigel, H., Eds.; Marcel Dekker: New York, 1998; Vol. 35, pp 239−328.
(5) Matzanke, B. F.; Müller-Matzanke, G.; Raymond, K. N. In *Iron Carriers and Iron Proteins*; Loehr, T. M., Ed.; VCH Publishers: New York, 1989; Vol. 5, pp 3−121.
(6) Neilands, J. B. *Annu. Rev. Biochem.* **1981**, *50*, 715−731.
(7) Raymond, K. N.; Telford, J. R. In *NATO ASI Series C, Mathematical and Physical Sciences*; Kessissoglous, D. P., Ed.; Kluwer Academic Publishers: Dordrecht, The Netherlands, 1995; Vol. 459, p 25.
(8) *Handbook of Microbial Iron Chelates*; Winkelmann, G., Ed.; CRC Press: Boca Raton, FL, 1991.

10.1021/ic0104003 CCC: $20.00
Published on Web 11/14/2001

membrane; and deposition at an appropriate site within the cell.[3,4,7] Microbial siderophores exhibit high and specific affinity for Fe(III) ($\log \beta > 30$)[4] to overcome the Fe(III) solubilization challenge. The Fe(III) siderophore complexes enter the bacterial cell through Ton B dependent outer membrane proteins that have high-affinity siderophore receptors to bind specific siderophore−iron complexes.[10−17] The iron release mechanism, the final step of siderophore-mediated microbial iron transport, still remains controversial primarily due to the high stability of Fe(III) siderophore complexes.[4] Four hypotheses regarding the iron release mechanism have been put forward: reduction of Fe(III),[18−21] ligand hydrolysis,[22,23] ternary complex formation[3,4,24] and ligand protonation.[25−28]

Extensive studies of enterobactin (Figure 1), the potent siderophore of enteric bacteria, and its metal complexes indicate that the chiral trilactone backbone and the spacer chain length are to some extent responsible for the high stability of the Fe(III) enterobactin complex and are critical in the receptor mediated transport and iron release mechanism.[9,13−16,18,22,23,25−34] The key steps of enterobactin-mediated iron transport are still not completely understood because the solution chemistry of enterobactin is complicated by the rapid hydrolysis of the trilactone backbone, the water insolubility of the uncharged triprotonated Fe(III) complex, and the air sensitivity of the catechol ring in basic conditions.[26,30] Synthetic analogues of enterobactin have been synthesized in which the trilactone backbone is substituted by a series of different scaffolds.[9,31−33,35−38] Such substitutions have been successful in avoiding the hydrolysis of the ester backbone, but in the process their water solubility was sacrificed as well as the chirality of the backbone. A chiral enterobactin analogue based on a *scyllo*-inositol scaffold has been synthesized,[39] and recently analogues with a *myo*-inositol scaffold have also been prepared.[40] However, enterobactin analogues based on a carbohydrate backbone have not yet been characterized with respect to their Fe(III) coordination chemistry.

A series of siderophore analogues have recently been synthesized based on a methyl α-D-glucopyranoside scaffold[41] with three catechol moieties per saccharide unit: the 6-trityl derivative of methyl 2,3,4-tris-*O*-{*N*-[2,3-di(hydroxy)benzoylglycyl]-aminopropyl}-α-D-glucopyranoside (H_6L_A) and the diacetoxy derivative of methyl 2,3,4-tris-*O*-{*N*-[2,3-di(hydroxy)benzoyl]-aminopropyl}-α-D-glucopyranoside (H_6L_B) (Figure 1). These compounds all show siderophore activity for certain bacterial strains.[41] Preliminary data[41] indicate that carbohydrates can substitute for the trilactone structure of enterobactin. The availability of different stereoisomeric forms of saccharides and their functional groups makes the carbohydrates particularly attractive for the design of model siderophores of variable structure and polarity, and the construction of an optimal octahedral binding cavity for the Fe(III) ion. The chiral saccharide backbone can provide favorable recognition and accessibility to cells, increase the hydrophilicity, and provide high hydrolytic stability. Such compounds and their physicochemical properties are of interest as they can be used as penetration vectors for antibiotics or other biological applications involving Fe(III) uptake and metabolism. Here we report the synthesis and solution characterization of the Fe(III) binding affinities of H_6L_A and H_6L_B.

Experimental Section

Materials. The methyl 2,3,4-tris-*O*-{*N*-[2,3-di(hydroxy)benzoylglycyl]-aminopropyl}-α-D-glucopyranoside (H_6L_A) was prepared from the 6-trityl derivative with boron trifluoride and the methyl 2,3,4-tris-*O*-{*N*-[2,3-di(hydroxy)benzoyl]-aminopropyl}-α-D-glucopyranoside (H_6L_B) from the corresponding diacetoxybenzoyl derivative by hydrolysis with sodium hydroxide under nitrogen in a procedure analogous to that reported elsewhere.[41]

H- and ^{13}C NMR spectra were recorded on a Bruker Advance DRX 300 and a Bruker Advance DPX 500 MHz spectrometer, respectively. The chemical shifts, δ, are given in parts per million. The coupling constants, J, are reported in hertz. High-resolution mass spectra were obtained by a Finnigan MAT 95 XV high-resolution mass spectrometer with electrospray ionization (ESI). Purification of the samples was carried out by preparative HPLC and was performed on an Abimed Gilson instrument equipped with a 115 UV detector (234 nm) and a Knauer Vertex reversed-phase column (250 × 32 mm) packed with Eurosper 100-C18 (7 mm). The column was eluted by a gradient of acetonitrile and water. The initial ratio of acetonitrile:water was 30:30 (v/v), and a final ratio of 100:0 (v/v) was achieved after a period of 25

(9) Loomis, L. D.; Raymond, K. N. *Inorg. Chem.* **1991**, *30*, 906−911.
(10) Braun, V.; Hantke, K.; Köster, W. In *Metal Ions in Biological Systems*; Sigel, A., Sigel, H., Eds.; Marcel Dekker: New York, 1998; Vol. 35, pp 67−145.
(11) Letain, T. E.; Postie, K. *Mol. Microbiol.* **1997**, *24*, 271−283.
(12) Postle, K. *Mol. Microbiol* **1990**, *4*, 2019−2025.
(13) Ecker, D. J.; Matzanke, B. F.; Raymond, K. N. *J. Bacteriol.* **1986**, *167*, 666−673.
(14) Ecker, D. J.; Loomis, L. D.; Cass, M. E.; Raymond, K. N. *J. Am. Chem. Soc.* **1988**, *110*, 2457−2464.
(15) Armstrong, S. K.; McIntosh, M. A. *J. Biol. Chem.* **1995**, *270*, 2483−2488.
(16) Newton, S. M. C.; Allen, J. S.; Cao, Z.; Qi, Z.; Jiang, X.; Sprencel, C.; Igo, J. D.; Foster, S. B.; Payne, M. A.; Klebba, P. E. *Proc. Natl. Acad. Sci. U.S.A.* **1997**, *94*, 4560−4565.
(17) van der Helm, D. In *Metal Ions in Biological Systems*; Sigel, A., Sigel, H., Eds.; Marcel Dekker: New York, 1998; Vol. 35, p 355−401.
(18) Hider, R. C.; Bickar, D.; Morrison, I. E. G.; Silver, J. *J. Am. Chem. Soc.* **1984**, *106*, 6983−6987.
(19) Barchini, E.; Cowart, R. E. *Arch. Microbiol.* **1996**, *166*, 51−57.
(20) Vartivarian, S. E.; Cowart, R. E. *Arch. Biochem. Biophys.* **1999**, *364*, 74−82.
(21) Yun, C.-W.; Ferea, T.; Rashford, J.; Ardon, O.; Brown, P. O.; Botstein, D.; Kaplan, J.; Philpott, C. C. *J. Biol. Chem.* **2000**, *275*, 10709−10715.
(22) Brickman, T. J.; McIntosh, M. A. *J. Biol. Chem.* **1992**, *267*, 12350−12355.
(23) O'Brien, I. G.; Cox, G. B.; Gibson, F. *Biochim. Biophys. Acta* **1971**, *237*, 537−549.
(24) Monzyk, B.; Crumbliss, A. L. *J. Inorg. Biochem.* **1983**, *19*, 19−39.
(25) Cass, M. E.; Garrett, T. M.; Raymond, K. N. *J. Am. Chem. Soc.* **1989**, *111*, 1677−1682.
(26) Pecoraro, V. L.; Harris, W. R.; Wong, G. B.; Carrano, C. J.; Raymond, K. N. *J. Am. Chem. Soc.* **1983**, *105*, 4623−4633.
(27) Pecoraro, V. L.; Wong, G. B.; Kent, T. A.; Raymond, K. N. *J. Am. Chem. Soc.* **1983**, *105*, 4617−4623.
(28) Raymond, K. N.; Cass, M. E.; Evans, S. *Pure Appl. Chem.* **1987**, *59*, 771−778.
(29) Matzanke, B.; Ecker, D. J.; Yang, T. S.; Huynh, B. H.; Muller, G.; Raymond, K. N. *J. Bacteriol.* **1986**, *167*, 674−680.
(30) Cohen, S. M.; Meyer, M.; Raymond, K. N. *J. Am. Chem. Soc.* **1998**, *120*, 6277−6286.
(31) Harris, W. R.; Carrano, C. J.; Cooper, S. R.; Sofen, S. R.; Avdeef, A.; McArdle, J. V.; Raymond, K. N. *J. Am. Chem. Soc.* **1979**, *101*, 6097−6104.
(32) Harris, W. R.; Raymond, K. N. *J. Am. Chem. Soc.* **1979**, *101*, 6534−6541.
(33) Rodgers, S. J.; Lee, C.-W.; Ng, C. Y.; Raymond, K. N. *Inorg. Chem.* **1987**, *26*, 1622−1625.
(34) Shanzer, A.; Libman, J. In *Handbook of Microbial Iron Chelates*; Winkelmann, G., Ed.; CRC Press: Boca Raton, FL, 1991; pp 309−338.
(35) Corey, E. J.; Hurt, S. D. *Tetrahedron Lett.* **1977**, 3923−3924.
(36) Weitl, F. L.; Raymond, K. N. *J. Am. Chem. Soc.* **1979**, *101*, 2728−2731.
(37) Akiyama, M.; Ikeda, T. *Chem. Lett.* **1995**, 849.
(38) Chimiak, A.; Neilands, J. B. *Struct. Bonding* **1984**, *58*, 89−96.
(39) Tse, B.; Kishi, Y. *J. Am. Chem. Soc.* **1993**, *115*, 7892−7893.
(40) Schnabelrauch, M.; Egbe, D. A. M.; Heinisch, L.; Reissbrodt, R.; Möllmann, U. *BioMetals* **1998**, *11*, 243−251.
(41) Heggemann, S.; Schnabelrauch, M.; Klemm, D.; Möllmann, U.; Reissbrodt, R.; Heinisch, L. *BioMetals* **2001**, *14*, 1.

min using a flux rate of 20 mL/min. Sample purity was determined by mass spectroscopic analysis.

Methyl 2,3,4-Tris-*O*-{*N*-[2,3-di(hydroxy)benzoyl-glycyl]-aminopropyl}-α-D-glucopyranoside (H_6L_A), $C_{43}H_{56}N_6O_{18}$ (944.96). Boron trifluoride etherate in methanol was added to a solution of methyl 2,3,4-tris-*O*-{*N*-[2,3-di(hydroxy)benzoyl-glycyl]-3-aminopropyl}-6-*O*-trityl-α-D-glucopyranoside[41] (330 mg, 0.27 mmol) in dichloromethane at room temperature. The reaction was monitored by TLC (3:1:0.5 chloroform−ethyl acetate−acetic acid) and was found to be completed after about 20 min. The reaction mixture was extracted three times with water, dried over Na_2SO_4, filtered, and evaporated in vacuo. The residue was purified by HPLC, and 160 mg (40% yield) of methyl 2,3,4-tris-*O*-{*N*-[2,3-di(hydroxy)benzoyl-glycyl]-aminopropyl}-α-D-glucopyranoside (H_6L_A) was obtained after lyophilization. $[\alpha]^{20}_D$: +32.0° (*c* 7.75, methanol). ^{1}H NMR (300 MHz, DMSO-d_6): 1.39−1.73 (m, 6H, $-CH_2-$), 2.95−4.43 (m, 27H, 6× CH 2−6, 3× OCH_2-, 3× $CO-CH_2-N$, 3× CH_2-N, $O-CH_3$), 4.73 (d, 1H, J = 3.2, CH1), 6.42−6.71 (m, 6H, aromatic CH), 6.83−7.31 (m, 3H, aromatic CH), 7.93 (b, 3H, NH), 8.34 (3H, NH), 8.64 (b, 3H, aromatic OH), 12,34 (b, 3H, aromatic OH). ^{13}C NMR (300 MHz, DMSO-d_6): 29.840, 30.013, 30.123 ($-CH_2-$), 35.953, 36.153, 36.351, ($-CH_2-N-$), 42.392, 42.458, 42.502 ($CO-CH_2-N$), 54.347 ($O-CH_3$), 60.204 (CH6), 67.856, 69.790, 70.654 ($O-CH_2-$), 71.336, 77.489, 79.987, 81.306 (CH2−5), 96.983 (CH1), 109.77, 110.47, 110.843, 112.89, 113.505, 113.874, 116.088, 116.374, 116.960, 117.253, 117.788, 118.007 (aromatic CH), 150.099, 150.773, 151.348, 151.853, 151.990, 152.749 (aromatic C−OH), 164.89, 165.126, 165.761 (CO), 168.725, 168.909, 168.321 (CO). MS (ESI): *m*/*z* 945.4 ($[M + H]^+$), 967.6 ($[M + Na]^+$).

Methyl 2,3,4-Tris-*O*-{*N*-[2,3-di(hydroxy)benzoyl]-aminopropyl}-α-D-glucopyranoside (H_6L_B), $C_{37}H_{47}N_3O_{15}$ (773.8). To a solution of sodium hydroxide (230 mg) in water (5 mL) methyl 2,3,4-tris-*O*-{*N*-[2,3-di(acetoxy)benzoyl]-aminopropyl}-α-D-glucopyranoside[41] (370 mg, 0.36 mmol) was added under N_2 atmosphere. The reaction mixture was stirred for 1 h and neutralized with 1 M HCl. A gray solid precipitated, which was filtered and washed with water. The residue was purified by HPLC, and 150 mg (17% yield) of methyl 2,3,4-tris-*O*-{*N*-[2,3-di(hydroxy)benzoyl]-aminopropyl}-α-D-glucopyranoside (H_6L_B) was obtained after lyophilization. $[\alpha]^{20}_D$ +38.4 (*c* 10.0, methanol). ^{1}H NMR (300 MHz, DMSO-d_6): 1.72−1.79 (m, 6H, $-CH_2-$), 3.12−3.19 (m, 2H, CH2, CH4),3.26 (s, 3H, α OCH_3), 3.28−3.43 (m, 6H, $-CH_2-N$), 3.49−3.53 (dd, 1H, J = 4.3, 12, CH6), 3.53−3.61 (m, 4H, OCH_2-), 3.63−3.68 (m,1H, CH6′), 3.73−3.78 (m, 2H, OCH_2-), 4,77 (d, 1H, J = 3.2, CH1), 6.61−6.67 (m, 3H, aromatic CH), 6.81−6.90 (m, 3H, aromatic CH), 7.23−7.27 (m, 3H, aromatic CH), 8.69 (b, 3H, NH), 9.07 (b, 3H, aromatic C−OH), 12,76 (b, 3H, aromatic C−OH). ^{13}C NMR (300 MHz, DMSO-d_6): 29.140, 29.792, 29.887 ($-CH_2-$), 36.425, 36.503, 36.596 ($-CH_2-N$), 54.259 ($O-CH_3$), 60.173 (CH6), 67.989, 69.845, 70.369 ($O-CH_2-$), 71.270 (CH3), 77.511 (CH4), 80.026 (CH2), 81.400 (CH5), 96.941 (CH1), 114.956, 117.071, 117.840, 118.745 (aromatic CH), 146.184, 149.611 (aromatic C−OH), 169.697 (CO). MS (ESI): *m*/*z* 774.5 ($[M + H]^+$), 796.4 ($[M + Na]^+$).

All solutions were prepared in deionized water. All pH measurements were made using a Corning 250 pH/ion meter equipped with an Orion ROSS pH electrode filled with 3.0 M NaCl solution. The pH was adjusted with NaOH or $HClO_4$ to obtain a neutral solution between 6.5 and 7.5. Stock solutions of 2.0 M $NaClO_4$ were prepared from solid sodium perchlorate hydrate (Aldrich 99+%) and standardized by passing through a Dowex 50 W-X8 strong acid cation-exchange column in H^+ form. The 2.0 M $HClO_4$ stock solution was prepared from concentrated perchloric acid (Fisher 70%) and standardized by titration with standard NaOH solution to the phenolphthalein end point. Fe(III) perchlorate stock solution (0.1 M) was prepared from recrystallized Fe(III) perchlorate (Aldrich), standardized spectrophotometrically in strong acid[42] and titrimetrically by reduction with Sn(II) and titrated with the primary standard potassium dichromate.[43] Carbonate free NaOH was prepared by diluting Fisher 1 M NaOH with deionized water purged with argon for 45 min and standardized by titration with standard 0.2000 M HCl from Fisher to the phenolphthalein end point.

Ligand solutions were prepared in deionized water. The tris-(catechol)iron(III) complexes were formed by adding 1 equiv of Fe(III) to the ligand solution and slowly increasing the pH to 10, with constant stirring over the course of 1 h.

Methods. Potentiometric Measurements. Samples (20.00 mL) were placed in a double-walled titration cell maintained at 25 ± 0.05 C by a circulating constant-temperature bath. Solutions were adjusted to 0.10 M ionic strength by the addition of 2.0 M $NaClO_4$, and all solutions were purged with argon prior to titration. A Titronic 96 standard buret was used for the titration; data were analyzed by the program SUPERQUAD.[44]

Spectrophotometric Measurements. UV−visible spectra were recorded using a Cary 100 spectrophotometer. All solutions were adjusted to 0.10 M ionic strength by the addition of $NaClO_4$. The UV−visible spectra of the iron complexes as a function of pH were obtained for a single solution. After each adjustment of pH, a visible spectrum was recorded; data were analyzed using the program LETAGROP-SPEFO.[45] In spectrophotometric competition experiments with EDTA, 5.0 mL samples were allowed to equilibrate for 24 h at 25 °C (24 h was deemed sufficient to reach equilibrium as spectra obtained after 72 h for selected samples showed no further change). Typical solutions were 1×10^{-4} M in Fe(III) and the ligand, with up to a 6-fold excess of EDTA (Aldrich). The protonation and Fe(III) formation constants for EDTA were taken from the critical compilation of Martell and Smith.[46]

Results and Discussion

Ligand pK_a Determination. Methyl 2,3,4-tris-*O*-{*N*-[2,3-di(hydroxy)benzoyl-glycyl]-aminopropyl}-α-D-glucopyranoside (H_6L_A) and methyl 2,3,4-tris-*O*-{*N*-[2,3-di(hydroxy)benzoyl]-aminopropyl}-α-D-glucopyranoside (H_6L_B) both display similar spectral shifts when they are titrated from pH 4 to 10. The initial maximum absorbance at high energy corresponding to lower pH gradually shifts to low energy, giving rise to two distinct isosbestic points as a function of increasing pH, an indication that the intensity of the peak increases upon deprotonation (Figure 2). This result is almost identical to the results obtained for enterobactin[9] and MECAM,[32] a synthetic enterobactin analogue. The titration experiments produced identical results when titrated in both directions, from low to high and from high to low pH, indicating complete reversibility of the reaction, and high acid and base stability for these triscatechol ligands based on a saccharide platform.

The potentiometric equilibrium curves for H_6L_A and H_6L_B and their Fe(III) complexes are shown in Figure 3. In this analysis both H_6L_A and H_6L_B are treated as six-proton systems and the parameter *a* plotted on the *x*-axis is the number of moles of base added per mole of ligand. Each ligand alone yielded titration curves with similar features. The ligand protonation constants, K_{H_n}, are defined by eq 2 and are listed in Table 1.

$$H_{n-1}L^{-7+n} + H^+ \overset{K_{H_n}}{\rightleftharpoons} H_nL^{-6+n} \quad (1)$$

$$K_{H_n} = \frac{[H_nL^{-6+n}]}{[H_{n-1}L^{-7+n}][H^+]} \quad (2)$$

(42) Bastian, R.; Weberling, R.; Palilla, F. *Anal. Chem.* **1956**, *28*, 459−462.
(43) Vogel, A. I. *Quantitative Inorganic Analysis Including Elementary Instrumental Analysis*, 3rd ed.; Longmans, Green and Co., Ltd.: London, 1968.
(44) Gans, P.; Sabatini, A.; Vacca, A. *J. Chem. Soc., Dalton Trans.* **1985**, 1195−1200.
(45) Sillen, L. G.; Warsquist, B. *Ark. Kemi* **1968**, *31*, 377−390.
(46) Martell, A. E.; Smith, R. M. *Critical Stability Constants*; Plenum Press: New York, 1974; Vol. 1.

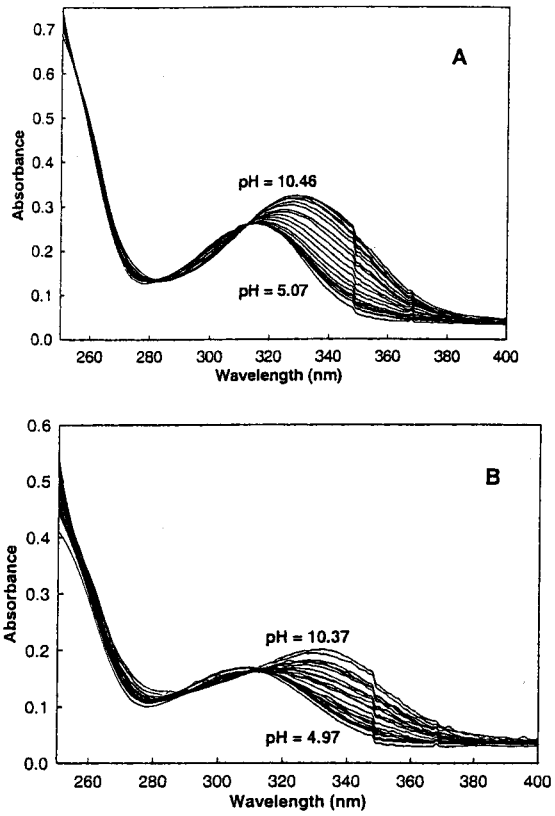

Figure 2. UV−visible spectra of (A) H_6L_A and (B) H_6L_B as a function of pH. Conditions: $[H_6L_A] = 1 \times 10^{-4}$ M, $[H_6L_B] = 0.9 \times 10^{-4}$ M; $\mu = 0.10$ M $NaClO_4$; $T = 298$ K.

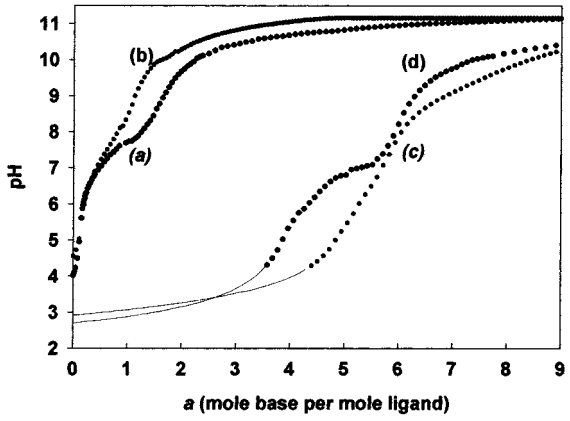

Figure 3. Potentiometric titration curves: (a) 5.0×10^{-4} M H_6L_A; (b) 4.9×10^{-4} M H_6L_B; (c) $H_6L_A + Fe^{3+}$, 1:1, 5.0×10^{-4} M; (d) $H_6L_B + Fe^{3+}$, 1:1, 4.9×10^{-4} M. The solid lines indicate precipitation. Conditions: $T = 298$ K and $\mu = 0.10$ M $NaClO_4$.

The lower three of these protonation constants (K_{H_n}; $n = 4-6$) are assigned to the more acidic ortho OH group on the catechol. The intrinsic acidity of the ortho hydroxide groups are higher relative to the meta hydroxy groups, and this is primarily due to the conjugation of the ortho hydroxy with the amide carbonyl.[47] The average log of the last three protonation constants for H_6L_B is 8.64, which is in very good agreement with the log of the lower protonation constant, 8.42, of *N*,*N*-dimethyl-2,3-dihydroxybenzamide.[31] However, the average log of the last three protonation constants for H_6L_A, 7.86, is much

Table 1. Ligand Protonation Constants for H_6L_A and H_6L_B[a]

	log K_{H_n}[b]	
n	H_6L_A	H_6L_B
1	12.9[c]	13.1[c]
2	12.1[c]	12.3[c]
3	11.3[c]	11.56 ± 0.22[d]
4	9.40 ± 0.16[d]	10.47 ± 0.21[d]
5	7.80 ± 0.24[d]	8.11 ± 0.27[d]
	7.82 ± 0.30[e]	
6	6.39 ± 0.31[d]	7.35 ± 0.25[d]

[a] Conditions: $T = 298$ K and $\mu = 0.10$ M $NaClO_4$. [b] Defined by eq 2. [c] Estimated on the basis of *N*,*N*-dimethyl-2,3-dihydroxybenzamide.[33,48] [d] Determined by potentiometric titration. [e] Determined by spectrophotometric titration.

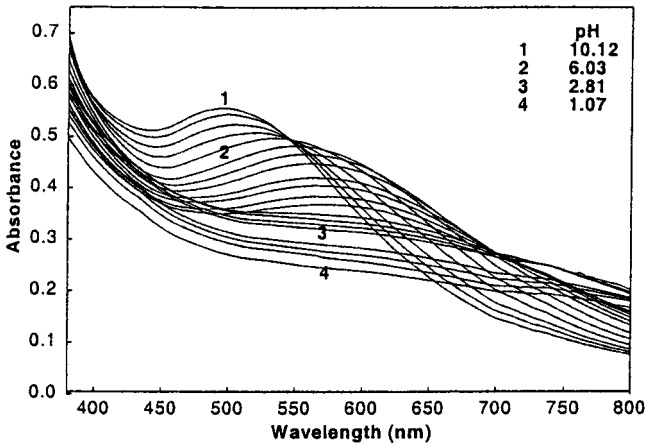

Figure 4. UV−visible spectra of Fe(III)−H_nL_A as a function of pH from pH 1.07 to 10.12. Conditions: $H_6L_A + Fe^{3+}$, 1:1, 1.25×10^{-4} M. $T = 298$ K and $\mu = 0.10$ M $NaClO_4$.

smaller than the log of the lower protonation constant of *N*,*N*-dimethyl-2,3-dihydroxybenzamide. This difference is attributed to the presence of a second amide carbonyl in the spacer chain that connects the saccharide scaffold to the catechol moieties, as the amide carbonyl groups are known to lower the protonation constants.[47] The first three protonation constants of H_6L_A and the first two protonation constants of H_6L_B were estimated on the basis of acidity differences between catechol and *N*,*N*-dimethyl-2,3-dihydroxybenzamide; the carbonyl group appears to lower the catechol protonation constant by 0.8 log unit.[48]

Fe(III) Complex Formation and Protonation Constants. General Considerations. The potentiometric titration curves for both ligands in the presence of equivalent concentrations of Fe(III) (Figure 3) show a clear inflection point at $a = 6$. At this point, both ligand solutions are deep red with $\lambda_{max} = 488$ nm ($\epsilon = 4610(9)$ M^{-1} cm^{-1}) for Fe(III)−H_6L_A and $\lambda_{max} = 484$ nm ($\epsilon = 5390(16)$ M^{-1} cm^{-1}) for Fe(III)−H_6L_B, which are assigned as the ligand-to-metal charge transfer (LMCT) bands.[49,50] These parameters and qualitative aspects of the UV−visible spectra are very similar to those corresponding to the tris Fe(III) complex of *N*,*N*-dimethyl-2,3-dihydroxybenzamide[51] and other tris(bidentate) model compounds that coordinate to Fe(III)

(47) Llinas, M.; Wilson, D. M.; Neilands, J. B. *Biochemistry* **1973**, *12*, 3836−3843.
(48) Raymond, K. N.; Müller, G.; Matzanke, B. F. In *Topics in Current Chemistry*; Boschke, F. L., Ed.; Springer-Verlag: Berlin, Heidelberg, 1984; Vol. 123, pp 49−102.
(49) Ballhausen, C. J. *Prog. Inorg. Chem.* **1960**, *2*, 251.
(50) Gordan, D. J.; Fenske, R. F. *Inorg. Chem.* **1982**, *21*, 2916−2923.
(51) Avdeef, A.; Sofen, S. R.; Bregante, T. L.; Raymond, K. N. *J. Am. Chem. Soc.* **1978**, *100*, 5362−5370.

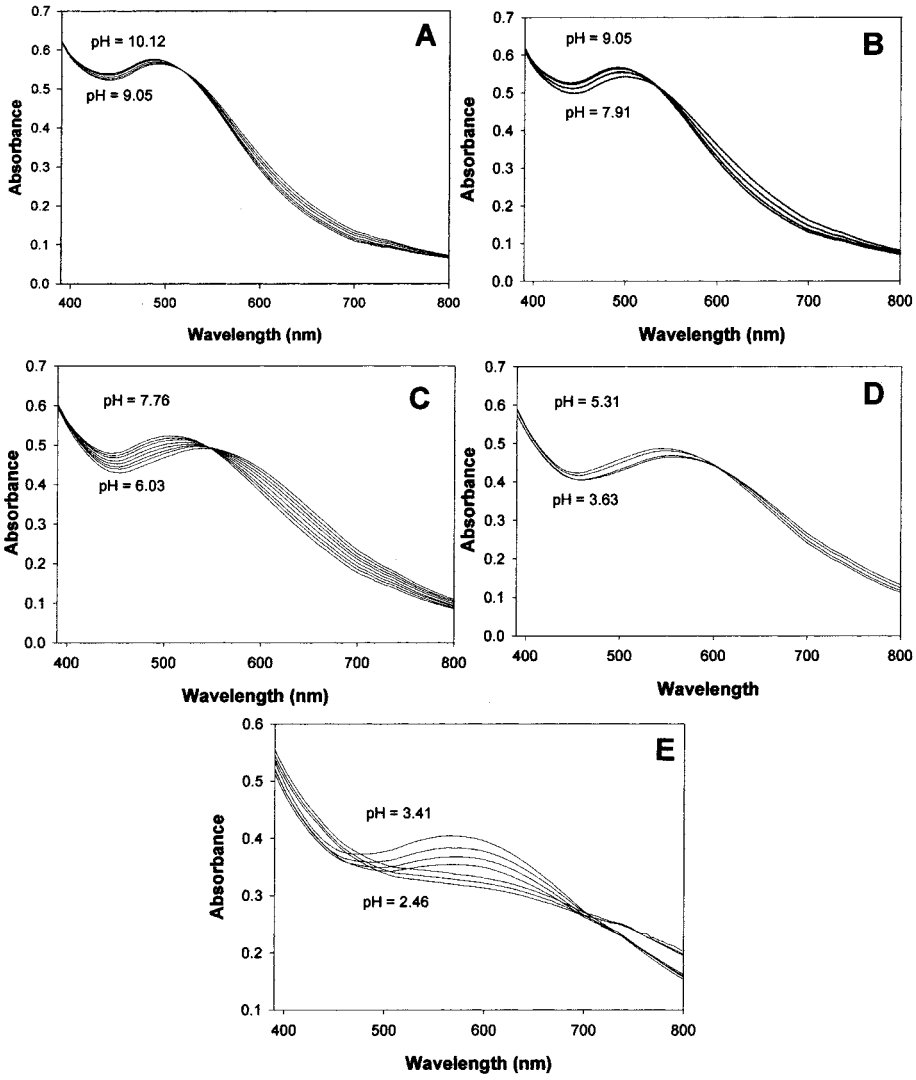

Figure 5. UV−visible spectra of Fe(III)−H_nL_A as a function of pH over different pH ranges showing different isosbestic points. Conditions: H_6L_A + Fe^{3+}, 1:1, 1.25×10^{-4} M. $T = 298$ K and $\mu = 0.10$ M $NaClO_4$.

through six phenolic oxygens.[52] Both the spectrophotometric and the potentiometric titrations indicate that at pH > 9.5 a single species is formed along with the displacement of six protons. Thus, the deep red complexes reported here can be identified as $Fe^{III}L_A^{3-}$ and $Fe^{III}L_B^{3-}$ with iron being coordinated through the six phenolic oxygen atoms of the three hydroxybenzoyl groups.

The titration curves of Fe(III)−H_6L_A and Fe(III)−H_6L_B are reliable only above pH 4.3 and 3.7, respectively, since below these pH values a dark purple precipitate was observed for both complexes. The precipitate in both cases redissolved to give a deep red solution when the pH was increased, over pH = 9.5, and regenerated the original spectra of $Fe^{III}L_A^{3-}$ and $Fe^{III}L_B^{3-}$ species. The purple precipitate is a neutral or insoluble iron species and not a degradation product of the reaction. This result is consistent with the observation made for the Fe(III)−MECAM interaction in aqueous media.[32]

$Fe^{III}L_A$ Protonation Constants. The potentiometric titration curve for H_6L_A in the presence of Fe(III) exhibits a gradual increase in the pH (Figure 3). This observation indicates successive deprotonation of Fe(III)−H_nL_A, giving the reaction mixture a buffering capability. The initially formed precipitate slowly dissolves over the course of the titration, and may also have contributed to the gradual pH increase by hindering the thorough mixing of the solution. The presence of the precipitate during titration prevented the use of the potentiometric data to obtain the protonation constants for the $Fe^{III}L_A^{3-}$ complex. However, the titration curve clearly indicates that the first three protonation constants for $Fe^{III}L_A^{3-}$ are well separated and lie between pH 4 and 7. The precipitation observed at lower pH during titration was eliminated by using a more dilute Fe(III)-complex solution for the spectrophotometric titration experiments discussed below.

The spectrophotometric titration allows us to determine the protonation constants by observing the changes in the intense LMCT band of the metal complex. The UV−visible spectra of Fe(III)−H_nL_A as a function of pH (Figure 4) have an overall shape similar to that for Fe(III)−*N*,*N*-dimethyl-2,3-dihydroxybenzamide,[51] a tris(bidentate) model compound. The isosbestic points at 546 and 704 nm are very similar to the isosbestic points observed for *N*,*N*-dimethyl-2,3-dihydroxybenzamide[51] of 543 and 688 nm. However, when the spectrophotometric titration was carried out very carefully in small [H^+] increments, five different isosbestic points were observed at 515 nm (pH 9.05−10.12), 534 nm (pH 7.91−9.05), 546 nm (pH 6.03−7.76), 605

(52) Gerard, C.; Chehhal, H.; Hugel, R. P. *Polyhedron* **1994**, *13*, 591−597.

Table 2. Protonation Constants for $Fe^{III}L^{3-}$ Complexes[a]

	log K_{MH_nL}[b]	
n	$Fe^{III}L_A^{3-}$	$Fe^{III}L_B^{3-}$
1	9.31 ± 0.07	10.12 ± 0.26
2	8.16 ± 0.16	9.12 ± 0.24
3	7.05 ± 0.19	7.59 ± 0.12
4	3.49 ± 0.09	5.72 ± 0.21
5	3.56 ± 0.19	5.25 ± 0.13

[a] Conditions: $T = 298$ K and $\mu = 0.10$ M $NaClO_4$. [b] As defined by eq 6.

nm (pH 3.63−5.31), and 704 nm (pH 2.46−3.41) (Figure 5). These isosbestic points indicate that over each indicated pH range a dominant equilibrium exists between two different metal complex species. This observation also explains the gradual pH increase that takes place during the potentiometric titration (Figure 3).

The first isosbestic point at 515 nm was treated as a one-proton step as indicated by eq 3, and the protonation constant K_{MHL} is defined by eq 4.

$$FeL_A^{3-} + H^+ \rightleftharpoons FeHL_A^{2-} \quad (3)$$

$$K_{MHL} = \frac{[FeHL_A^{2-}]}{[FeL_A^{3-}][H^+]} \quad (4)$$

The following four isosbestic points were also treated as sequential one-proton steps. The corresponding equilibria are represented by eq 5 and the protonation constants are defined by eq 6, respectively ($n = 1-6$).

$$FeH_{n-1}L_A^{-4+n} + H^+ \rightleftharpoons FeH_nL_A^{-3+n} \quad (5)$$

$$K_{MH_nL} = \frac{[FeH_nL_A^{-3+n}]}{[FeH_{n-1}L_A^{-4+n}][H^+]} \quad (6)$$

The protonation constants for the $Fe^{III}L_A^{3-}$ complex were calculated by refining the entire spectrophotometric data set using the program LETAGROP-SPEFO[45] to fit the above-described model. This model fits the data well as indicated by the small standard deviations for the protonation constants tabulated in Table 2. The first three protonation constants are well separated as indicated by the potentiometric results. The presence of precipitate, at lower pH, during titration resulted in an overall decrease in the spectral absorbance, and thus the sixth protonation constant could not be refined.

$Fe^{III}L_B$ Protonation Constants. The potentiometric titration curve for Fe(III)−H_6L_B (Figure 3) is similar but steeper compared to the Fe−H_6L_A titration curve, indicating a tighter Fe(III) binding capability over H_6L_A. Similar to the Fe(III)−H_6L_A complex, precipitation was observed at pH 3.7, which prevented the use of potentiometric data to calculate the protonation constants. The two two-proton buffer regions, however, indicate that the first two protonation constants and the fourth and fifth protonation constants are very close to each other.

The results of the spectrophotometric titration for Fe(III)−H_6L_B (Figure 6) are very similar to those for Fe(III)−H_6L_A, as well as the tris Fe(III) complex of *N*,*N*-dimethyl-2,3-dihydroxybenzamide.[51] Similar to the Fe(III)−H_6L_A spectra, when the spectrophotometric titration was carried out in small $[H^+]$ increments, five different isosbestic points were observed at 491 nm (pH 9.85−11.17), 526 nm (pH 8.52−9.56), 556 nm (pH 7.22−8.19), 571 nm (pH 5.49−6.97), and 682 nm (pH 3.82−4.70) (Figure 7). The two isosbestic points at 556 and 682 nm are very similar to the isosbestic points observed for *N*,*N*-dimethyl-2,3-dihydroxybenzamide of 543 and 688 nm.[51] These isosbestic points occur over a narrower wavelength range than those observed for the Fe(III)−H_6L_A system, and they also indicate that over each narrow pH range shown in Figure 7 a dominant proton-driven equilibrium exists between two different metal complex species.

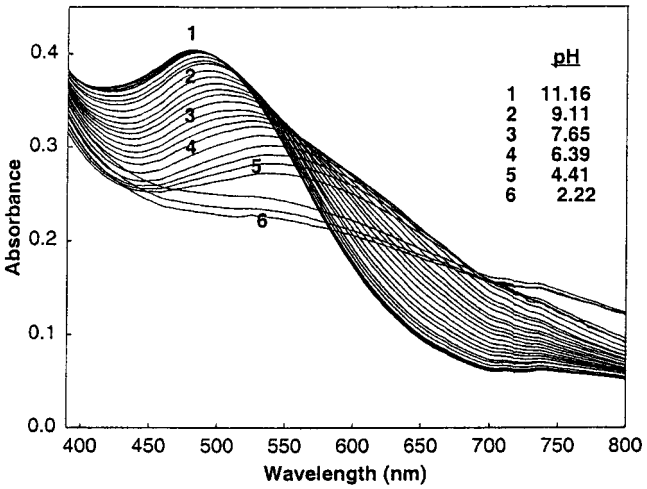

Figure 6. UV−visible spectra of Fe(III)−H_nL_B as a function of pH from pH 2.22 to 11.16. Conditions: H_6L_B + Fe^{3+}, 1:1, 7.59×10^{-5} M. $T = 298$ K and $\mu = 0.10$ M $NaClO_4$.

The spectrophotometric titration data for Fe(III)−H_6L_B were refined using the same assumptions as used for Fe(III)−H_6L_A. Each isosbestic point was treated as a simple equilibrium between two different species, and the protonation constants were calculated by refining the entire spectrophotometric titration data set using the same model described earlier for the $Fe^{III}L_A^{3-}$ system. This model fits the data well as demonstrated by the standard deviations for the protonation constants tabulated in Table 2. As indicated by the potentiometric results, the first two and the last two protonation constants are fairly close to each other, and for reasons similar to those for the $Fe^{III}L_A^{3-}$ system, the sixth protonation constant could not be refined.

Overall Complex Stability and Species Distribution. The protonation constants that were determined for $Fe^{III}L_A^{3-}$ and $Fe^{III}L_B^{3-}$ were used to generate a species distribution curve (Figure 8). The speciation diagram for both the Fe(III)−H_6L_A and Fe(III)−H_6L_B systems clearly show $Fe^{III}H_3L$ as the most abundant species over a relatively large pH range. It is probable that these neutral species are formed due to a salicylate mode of binding[30] shown below.

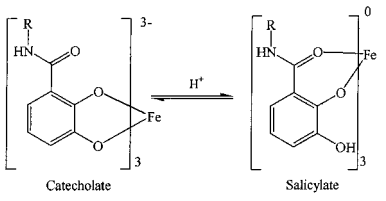

The overall stability constants, log β_{110} (defined by eq 8), for both $Fe^{III}L_A^{3-}$ and $Fe^{III}L_B^{3-}$ were calculated using the program LETAGROP-SPEFO[45] and were found to be in good agreement with those calculated for similar synthetic

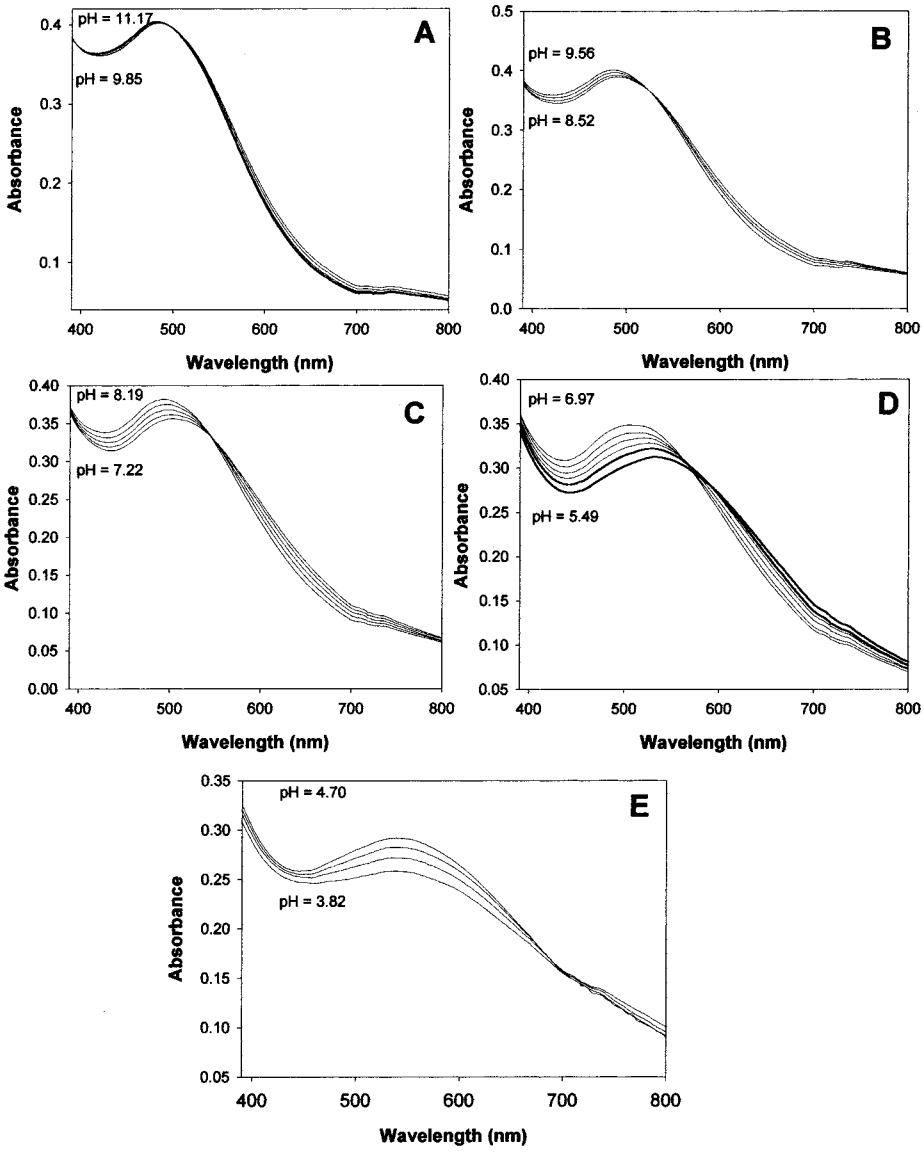

Figure 7. UV−visible spectra of Fe(III)−H_nL_B as a function of pH over different pH ranges showing different isosbestic points. Conditions: H_6L_B + Fe^{3+}, 1:1, 7.59×10^{-5} M. $T = 298$ K and $\mu = 0.10$ M $NaClO_4$.

enterobactin analogues (Table 3).[31−33] The equilibrium is represented by eq 7,

$$Fe_{aq}^{3+} + L^{6-} \rightleftharpoons FeL^{3-} \tag{7}$$

$$\beta_{110} = \frac{[FeL^{3-}]}{[Fe_{aq}^{3+}][L^{6-}]} \tag{8}$$

where L represents the ligands L_A^{6-} and L_B^{6-}.

The stability of the Fe(III) complexes of H_6L_A and H_6L_B was also determined by spectrophotometric competition experiments with EDTA at pH 9.9 for H_6L_A and at pH 9.7 for H_6L_B. The competition equilibrium is described by eqs 9 and 10,

$$Fe^{III}EDTA + L \overset{K}{\rightleftharpoons} Fe^{III}L + EDTA \tag{9}$$

$$K = \frac{[Fe^{III}L][EDTA]}{[Fe^{III}EDTA][L]} = \frac{\beta_{110}^{FeL}}{\beta_{110}^{FeEDTA}} \tag{10}$$

where L represents the ligands H_6L_A and H_6L_B, and molecular charges and water molecules involved in the equilibrium are omitted for clarity. The concentrations of $Fe^{III}L_A^{3-}$ and $Fe^{III}L_B^{3-}$ were calculated from the absorbance at 488 and 484 nm respectively, where $Fe^{III}L^{3-}$ is the only light-absorbing species. The concentrations of other species in eq 10 were calculated from mass balance equations using the experimental pH values,

$$[Fe]_{tot} = \alpha_{Fe^{III}L}[Fe^{III}L] + \alpha_{Fe^{III}EDTA}[Fe^{III}EDTA] \tag{11}$$

$$[L]_{tot} = \alpha_{Fe^{III}L}[Fe^{III}L] + \alpha_{L}[L] \tag{12}$$

$$[EDTA]_{tot} = \alpha_{Fe^{III}EDTA}[Fe^{III}EDTA] + \alpha_{EDTA}[EDTA] \tag{13}$$

where α is the usual Ringbom's coefficient.[53] The stability constants, log β_{110}, for Fe(III)L_A^{3-} and Fe(III)L_B^{3-} were calculated using the relationship defined by eq 10 and were found to be 41.2 and 46.1, respectively, which are in excellent

(53) Ringbom, A. *Complexation in analytical chemistry; a guide for the critical selection of analytical methods based on complexation reactions*; Interscience Publishers: New York, 1963.

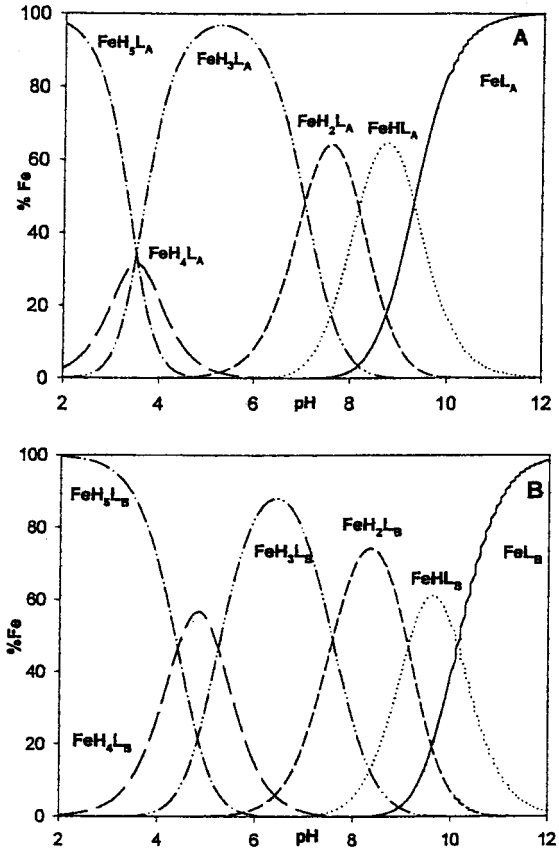

Figure 8. Calculated species distribution for Fe(III) complexes of (A) H_6L_A and (B) H_6L_B. Metal-containing species are normalized to the total concentration of Fe(III). Conditions: $H_6L_A/H_6L_B + Fe^{3+}$, 1:1. $T = 298$ K and $\mu = 0.10$ M $NaClO_4$.

Table 3. Fe(III) Complex Stability Constants[a]

ligand	log β_{110}[b]	pFe[c]	ref
H_6L_A	41.38 ± 0.11	28.6 ± 0.7	this work
H_6L_B	46.38 ± 0.26	28.3 ± 0.9	this work
MECAM	46	29.1	31, 32
TRENCAM	43.6	27.8	33
CYCAM	40	23.0	32
enterobactin	49	35.5	9

[a] Determined by spectrophotometric titration. Conditions: $T = 298$ K and $\mu = 0.10$ M $NaClO_4$. [b] Defined by eq 8. [c] $-\log [Fe^{3+}]$ at $[Fe(III)]_{tot} = 10^{-6}$ M, $[ligand]_{tot} = 10^{-5}$ M and pH = 7.4.

agreement with the values determined from the spectrophotometric titrations.

In order to compare the Fe(III) binding properties of ligands H_6L_A and H_6L_B with other Fe(III) chelators at physiological conditions, the pFe values were calculated ($-\log[Fe^{3+}]$ at pH = 7.4 with the total ligand concentration ($[L]_{tot}$) 10^{-5} M and a total Fe(III) concentration of 10^{-6} M).[48] The concentration of free Fe(III) ion in solution can be expressed by eq 14. The pFe

$$[Fe(III)] = \frac{[FeL]_{tot}}{\beta_{110}[(L)_{tot} - (FeL)_{tot}]} = \frac{\alpha L}{9(\alpha FeL)\beta_{110}} \quad (14)$$

values for H_6L_A and H_6L_B were calculated to be 28.6 ± 0.7 and 28.3 ± 0.9, respectively. Both of these values are comparable to or greater than the values calculated for similar synthetic analogues (Table 3)[9,31−33] and are significantly higher than that of transferrin, 23.6.[31]

Siderophore Activity. The biological activity of H_6L_A and H_6L_B was examined by growth promotion tests involving bioassays of various bacteria with a well-defined ability to transport and utilize natural siderophores (siderophore indicator strains)[54] as well as wild-type strains. Both H_6L_A and H_6L_B displayed good growth promotion (siderophore) activity. In general, H_6L_B exhibited somewhat higher growth-promoting activity than H_6L_A. The details are reported separately.[41] These results are consistent with the high binding affinity of both H_6L_A and H_6L_B for Fe(III). The log β_{110} for H_6L_B is greater than for H_6L_A, in parallel with the small difference in growth activity for the two ligands. However, since the pFe values for H_6L_A and H_6L_B are the same, differences in biological activity is more likely due to difference in speciation. At pH 7 ca. 80% of the H_6L_B/Fe(III) system is in the form of neutral complex (FeH_3L_B), while ca. 50% of the H_6L_A/Fe(III) system is present as the neutral FeH_3L_A. Formation of an uncharged complex may favor membrane permeability and cellular uptake.

Summary and Conclusions

The Fe(III) coordination chemistry of two enterobactin analogues, methyl 2,3,4-tris-*O*-{*N*-[2,3-di(hydroxy)benzoyl-glycyl]-aminopropyl}-α-D-glucopyranoside (H_6L_A) and methyl 2,3,4-tris-*O*-{*N*-[2,3-di(hydroxy)benzoyl]-aminopropyl}-α-D-glucopyranoside (H_6L_B), with a chiral saccharide backbone were explored in aqueous solution. The thermodynamic and the spectroscopic properties of the Fe(III) complexes closely parallel those of Fe[enterobactin]$^{3-}$ and Fe(III) complexes of other synthetic enterobactin analogues. The Fe(III) binding affinities of H_6L_A and H_6L_B are equivalent to or better than that reported for other enterobactin models. Growth promotion tests for both H_6L_A and H_6L_B indicate significant siderophore activity. These thermodynamic and spectroscopic similarities along with the chiral saccharide backbone and siderophore activity of H_6L_A and H_6L_B make these ligands very attractive to investigate as substrates for receptor proteins that recognize the Fe(III) complex of enterobactin.

Acknowledgment. We thank the National Science Foundation (A.L.C.) for financial support.

IC0104003

(54) Reissbrodt, R.; Heinisch, L.; Möllmann, U.; Rabsch, W.; Ulbricht, H. *BioMetals* **1993**, *6*, 155−162.